HHS Public Access

Author manuscript

Biochemistry. Author manuscript; available in PMC 2017 August 21.

Published in final edited form as:

Biochemistry. 2017 February 21; 56(7): 903–906. doi:10.1021/acs.biochem.6b01237.

Confinement and Stabilization of Fyn SH3 Folding Intermediate Mimetics within the Cavity of the Chaperonin GroEL Demonstrated by Relaxation-Based NMR

David S. Libich[†], **Vitali Tugarinov**[†], **Rodolfo Ghirlando**[‡], and **G. Marius Clore**[*,†]

[†]Laboratory of Chemical Physics, National Institute of Diabetes and Digestive and Kidney Diseases, National Institutes of Health, Bethesda, Maryland 20892-0520, United States

[‡]Laboratory of Molecular Biology, National Institute of Diabetes and Digestive and Kidney Diseases, National Institutes of Health, Bethesda, Maryland 20892-0520, United States

Abstract

The interaction of two folding intermediate mimetics of the model protein substrate Fyn SH3 with the chaperonin GroEL, a supramolecular foldase/unfoldase machine, has been investigated by ^{15}N relaxation-based nuclear magnetic resonance spectroscopy (lifetime line broadening, dark state exchange saturation transfer, and relaxation dispersion). The two mimetics comprise C-terminal truncations of wild-type and triple-mutant (A39V/N53P/V55L) Fyn SH3 in which the C-terminal strand of the SH3 domain is unfolded, while preserving the remaining domain structure. Quantitative analysis of the data reveals that a mobile state of the SH3 domain confined and tethered within the cavity of GroEL, possibly through interactions with the disordered, methionine-rich C-terminal tail(s), can be detected, and that the native state of the folding intermediate mimetics is stabilized by both confinement within and binding to apo GroEL. These data provide a basis for understanding the passive activity of GroEL as a foldase/unfoldase: the unfolded state, in the absence of hydrophobic GroEL-binding consensus sequences, is destabilized within the cavity because of its larger radius of gyration compared to that of the folding intermediate, while the folding intermediate is stabilized relative to the native state because of exposure of a hydrophobic patch that favors GroEL binding.

GroEL is a large (800 kDa) supramolecular machine that facilitates protein folding and protects against the damaging effects of misfolding and aggregation.[1] GroEL comprises two heptameric rings, each of which encloses a large cavity accessible to protein substrates. The mechanism whereby GroEL exerts its effect encompasses a series of concerted allosteric

[*]Corresponding Author: mariusc@mail.nih.gov.

ORCID

G. Marius Clore: 0000-0003-3809-1027

Author Contributions

D.S.L. and V.T. contributed equally to this work.

The authors declare no competing financial interest.

Supporting Information

The Supporting Information is available free of charge on the ACS Publications website at DOI: 10.1021/acs.biochem. 6b01237.

Details of sample preparation, NMR experiments, and fitting of the experimental data (Figures S1–S9) (PDF)

transitions driven by the hydrolysis of ATP and the binding and dissociation of the co-chaperonin GroES that caps the open rings of GroEL. Apo GroEL, however, can also function as a passive anti-aggregation chamber as evidenced by both H/D and fluorescence-based folding experiments.[2] Recently, we presented a quantitative study of the interaction of a model, metastable SH3 domain with apo GroEL[3] by combined analysis of ^{15}N Carr–Purcell–Meiboom–Gill (CPMG) relaxation dispersion,[4] dark state exchange saturation transfer (DEST),[5] and lifetime line broadening (ΔR_2)[6] nuclear magnetic resonance (NMR) experiments.[7] The model domain consisted of a triple (A39V/N53P/V55L) mutant of Fyn SH3 (SH3^{Mut}) that, at a low temperature (10 °C), exists in equilibrium between the major native state (F) and a sparsely populated (~2%) folding intermediate (I) in which the C-terminal β-strand is disordered, exposing a hydrophobic patch.[8] We showed that apo GroEL stabilizes the folding intermediate, accelerates the overall interconversion between the two states ~20-fold, and increases the rate constant for the F to I transition by ~500-fold.[3] In this paper, we investigate two mimetics of the folding intermediate, one stable and the other metastable, and present NMR evidence of confinement and stabilization of the folding intermediate mimetics within the cavity of apo GroEL.

The two mimetics of the Fyn SH3 folding intermediate comprise three-residue (SH3^{WT}Δ57) and four-residue (SH3^{Mut}Δ56) C-terminal truncations of the full-length wild-type and triple-mutant domains, respectively (see the Supporting Information for full details of cloning, expression, and purification). The ^{1}H–^{15}N correlation spectra of SH3^{Mut}Δ56 and SH3^{WT}Δ57 are well-resolved and characteristic of folded proteins (Figure S1). The global folds for both truncated constructs, determined using CS-Rosetta[9] from backbone chemical shifts and residual dipolar couplings (Figure S2), are very similar to one another (Figure 1A) as well as to the native and folding intermediate states of full-length SH3^{Mut} (Figure S3). The distinguishing characteristic of both truncation mutants and the folding intermediate[8] of full-length SH3^{Mut} is the unfolding of the C-terminal β-strand; the remaining domain structure, however, remains essentially unchanged relative to the native state. Analytical ultra-centrifugation (Figure S4) and ^{15}N CPMG relaxation dispersion measurements (Figure S5) show that the folded (F) monomeric state of SH3^{Mut}Δ56 undergoes concentration-dependent exchange with a folded dimer (F_D) and concentration-independent exchange with the fully unfolded (U) state, while SH3^{WT}Δ57 is a stable folded monomer with no significant relaxation dispersion ($R_{ex} < 1\ s^{-1}$). For SH3^{Mut}Δ56, for which large dispersions are observed, the calculated ^{15}N chemical shifts for the unfolded state are fully consistent with those predicted for a random coil (Figure S5B); in addition, five residues have optimized values of >0.7 ppm for the ^{15}N chemical shift differences between folded monomeric and dimeric states (Figure S5C). The latter, together with residues showing severely broadened ^{1}H/^{15}N correlations at a high concentration of SH3^{Mut}Δ56, form a single contiguous dimerization interface that largely coincides with the hydrophobic GroEL-binding surface[3] (Figure S6).

In the presence of apo GroEL, relatively uniform ^{15}N lifetime line broadening is observed for both SH3^{Mut}Δ56 (Figure 1B) and SH3^{WT}Δ57 (Figure S7A), which is largely abolished when the cavity of GroEL is blocked by acid-denatured Rubisco (Figure 1B), a protein substrate that binds with nanomolar affinity to GroEL.[11] Significant broadening of ^{15}N DEST profiles is also observed for both SH3^{Mut}Δ56 (Figure 2A) and SH3^{WT}Δ57 (Figure

S7B) in the presence of apo GroEL with widths at half-height of ~5 kHz at saturation field strengths of 500–750 Hz. No significant relaxation dispersions are observed for $SH3^{WT}\Delta57$ in the presence of apo GroEL, indicating that any unfolded GroEL-bound species remains below the level of detection. Thus, one can conclude that the ΔR_2 and DEST effects arise from the binding of the folded truncated species to the high-molecular weight apo GroEL (presumably at the apical domain). The magnetic field dependence of ΔR_2 is smaller than that expected for a relaxation mechanism based on the one-bond ^1H–^{15}N dipolar coupling interaction and a −170 ppm ^{15}N chemical shift anisotropy: $\Delta R_2^{900}/\Delta R_2^{600}=1.08\pm0.08$ for $SH3^{Mut}\Delta56$ (Figure 1B) and $\Delta R_2^{800}/\Delta R_2^{600}=1.14\pm0.06$ for $SH3^{WT}\Delta57$ (Figure S7A) compared to expected values of 1.3 and 1.2, respectively, indicating that exchange is in the slow-to-intermediate exchange regime on the relaxation time scale and the overall value of the pseudo-first-order rate constant for exchange between small (observable) and high-molecular weight “dark” species is close to the maximal value of ΔR_2.[5,6]

The ^{15}N CPMG dispersion profiles for $SH3^{Mut}\Delta56$ in the presence of apo GroEL are characterized by a decrease in R_{ex} (i.e., the difference in $R_{2,eff}$ between the lowest and highest CPMG field strengths) relative to those for free $SH3^{Mut}\Delta56$ (Figure 2B). This is manifested by only a small increase in $R_{2,eff}$ at the lowest CPMG field, while at high CPMG fields (1000 Hz), $R_{2,eff}$ is increased by ~ΔR_2. The reduction in R_{ex} is eliminated when GroEL is blocked by acid-denatured Rubisco (Figure S8). Direct binding of the folded state (F) to GroEL (i.e., exchange with a slowly tumbling species) cannot by itself lead to a decrease in R_{ex}. To explain this observation, an additional observable state (F_E) that does not exchange with unfolded state U in the presence of GroEL has to be invoked in which the folded conformation is tethered and stabilized upon confinement within the cavity of GroEL (Figure 3). In effect, the presence of state F_E reduces the population of the species that can spontaneously unfold with a concomitant decrease in R_{ex}. The confined state F_E is considered to be an observable state with the same ^{15}N chemical shifts and R_2 values comparable to those of F.

The full kinetic scheme describing all possible equilibria in the $SH3^{Mut}\Delta56$/GroEL system is shown in Figure 3. The folded state F is in slow exchange with unfolded state U and the dimeric form of the protein (F_D) in bulk solution. Observable folded (F_E) and unfolded (U_E) states confined within the GroEL cavity reorient rapidly; the corresponding “dark”, directly bound species, F_B and U_B, tumble with the same rotational correlation time as GroEL. In addition, both confined and directly bound species can potentially undergo inter-conversion between folded and unfolded states. The maximal possible fraction of U_E, in the absence of stabilization of F_E, is <1% as free unfolded species U is sparsely populated. If the $F_E \leftrightarrow U_E$ interconversion is even slightly shifted toward F_E, the fraction of U_E becomes even smaller. Initial fitting of all the relaxation data (see the Supporting Information for full details of the fitting) to the full model shown in Figure 3 (including the parts colored light gray) indicated that the populations of U_E and U_B could not be defined and were driven to zero during minimization. We therefore conclude that states U_E and U_B are undetectable because of their very small populations (consistent with the absence of any sequential, hydrophobic GroEL-binding consensus sequences[12]), which, in effect, is equivalent to assuming that unfolding of $SH3^{Mut}\Delta56$ does not occur within the GroEL cavity. Thus, the five-state model given by the

states colored black in Figure 3 can fully account for the relaxation data for the $SH3^{Mut}\Delta56$/GroEL system.

The complexity of the kinetic scheme in Figure 3 precludes the definition of all the rate constants. In addition, the population (p_B) and average R_2 value of F_B are correlated in the slow-to-intermediate exchange regime so that p_B can be defined only by assuming a value of $\langle {}^{15}N - R_{2,F_B} \rangle$ consistent with the molecular weight (~800 kDa) of GroEL [~950 s^{-1} at 900 MHz and 10 °C (Supporting Information and Figure S9)]. This allows one to define the populations of the F_E (~21%) and F_B (~2.6%) states, as well as the overall rate constants for the interconversion of the F and F_B states through direct ($F \leftrightarrow F_B$) and indirect ($F \leftrightarrow F_E \leftrightarrow F_B$) pathways; the relative contributions of these two pathways, however, cannot be determined. The overall rate constants for the conversion of F to F_B and the reverse F_B to F process are given by[13]

$$k_{on}^{overall} = k_{F \to B} + k_{F \to E \to B} = k_{FB} + k_{FE} k_{EB} / (k_{EF} + k_{EB})$$

and

$$k_{off}^{overall} = k_{B \to F} + k_{B \to E \to F} = k_{BF} + k_{EF} k_{BE} / (k_{EF} + k_{EB})$$

with values in the range 4–6 and 100–160 s^{-1}, respectively. (Note the small population of the "dark" F_B state is fully consistent with the observation that no measurable reduction in cross-peak volumes can be detected in the ^1H–^{15}N correlation spectrum of $SH3^{Mut}\Delta56$ in the presence of GroEL.)

The population of the confined state F_E corresponds to an occupancy of approximately one molecule of $SH3^{Mut}\Delta56$ per cavity. Given a cavity volume of ~85000 Å,[3,14] the concentration of F_E within the cavity is ~20 mM, corresponding to a 200-fold enrichment relative to the concentration in the bulk solution (100 μM). The simplest explanation for this phenomenon is that the F_E state of $SH3^{Mut}\Delta56$ is tethered to the end of one or more of the 23-residue, methionine-rich C-terminal tails (each containing five methionines in the last 11 residues of the sequence). Because the tails are intrinsically disordered (invisible in the apo GroEL electron density map)[10,14] and highly mobile [as evidenced by a set of very sharp, superimposed, methionine methyl cross-peaks at the random coil position in a ^1H–^{13}C TROSY correlation spectrum of a [$^{13}C_{methyl}$]methionine-labeled sample (unpublished data)], the effective rotational correlation time and hence R_2 values of F_E would be very similar to those of the F state in bulk solution.

Why is the folded state of $SH3^{Mut}\Delta56$ stabilized within the GroEL cavity? The radius of gyration (R_{gyr}) of fully unfolded $SH3^{Mut}\Delta56$ is estimated to be 20–24 Å.[15] The radius of the cylindrical cavity of GroEL is ~30 Å.[10,14] Thus, one would predict, from purely entropic considerations, that the folded state of $SH3^{Mut}\Delta56$ (R_{gyr} ~ 12–14 Å) would be preferred over the fully unfolded state upon confinement in the GroEL cavity in the absence of any compensatory interactions of the unfolded state with the cavity walls.[16] Using the random-

flight Gaussian chain model developed by Zhou and Dill[17] to describe the thermodynamics of stabilization of protein folded states upon confinement within a cavity, the energy of stabilization ($\Delta\Delta G$) for folded $SH3^{Mut}\Delta56$ is calculated to be −2.2 kcal mol^{-1}, corresponding to a population of ~0.017% for the confined unfolded state U_E (Figure 3A) (see the Supporting Information). Such small fractions cannot be detected by relaxation-based NMR techniques and can be safely neglected in analysis. In addition, numerical simulations of relaxation dispersion profiles for the full system in Figure 3 (encompassing a total of seven exchanging states) show that the lower bound for the fraction of U_E detectable under the experimental conditions used in this work is approximately 0.2–0.3%.

In conclusion, through the combined analysis of ^{15}N lifetime line broadening, DEST, and CPMG relaxation dispersion, we have shown that protein substrates can be confined and tethered within the cavity of GroEL (probably through interaction with the disordered C-terminal tails) and that the folding intermediate of the Fyn SH3 domain, represented by the $SH3^{Mut}\Delta56$ truncation mutant, is stabilized upon confinement within the GroEL cavity relative to the unfolded state. In conjunction with our previous work[3] on the interaction of $SH3^{Mut}$ with GroEL, we have now obtained a more complete picture of the passive effect that GroEL exerts on these particular protein substrates. Specifically, GroEL stabilizes folding intermediates relative to both folded (in the case of $SH3^{Mut}$) and unfolded (in the case of $SH3^{Mut}\Delta56$) states and, in addition, increases the rate of interconversion between fully folded and folding intermediate states. The unfolded state of the SH3 domain, which does not contain any hydrophobic GroEL consensus binding sequences,[12] is disfavored within the GroEL cavity because of its larger radius of gyration, while the folding intermediate is favored over the native state by exposure of a GroEL binding-competent hydrophobic patch upon unfolding of the C-terminal $\beta5$ strand of the SH3 domain.

Supplementary Material

Refer to Web version on PubMed Central for supplementary material.

Acknowledgments

Funding

This work was supported by the Intramural Program of NIDDK, NIH, and by the AIDS Targeted Antiviral program of the Office of the Director of the NIH (to G.M.C.).

We thank Drs. Baber, Garrett, and Ying for technical support.

References

1. (a) Thirumalai D, Lorimer GH. Annu Rev Biophys Biomol Struct. 2001; 30:245–269. [PubMed: 11340060] (b) Horwich AL, Fenton WA. Q Rev Biophys. 2009; 42:83–116. [PubMed: 19638247] (c) Hartl FU, Bracher A, Hayer-Hartl M. Nature. 2011; 475:324–332. [PubMed: 21776078]
2. (a) Robinson CV, Gross M, Eyles SJ, Ewbank JJ, Mayhew M, Hartl FU, Dobson CM, Radford SE. Nature. 1994; 372:646–651. [PubMed: 7990955] (b) Zahn R, Spitzfaden C, Ottiger M, Wuthrich K, Pluckthun A. Nature. 1994; 368:261–265. [PubMed: 7908413] (c) Zahn R, Perrett S, Stenberg G, Fersht AR. Science. 1996; 271:642–645. [PubMed: 8571125] (d) Zahn R, Perrett S, Fersht AR. J Mol Biol. 1996; 261:43–61. [PubMed: 8760501] (e) Priya S, Sharma SK, Sood V, Mattoo RU,

Finka A, Azem A, De Los Rios P, Goloubinoff P. Proc Natl Acad Sci U S A. 2013; 110:7199–7204. [PubMed: 23584019]

3. Libich DS, Tugarinov V, Clore GM. Proc Natl Acad Sci U S A. 2015; 112:8817–8823. [PubMed: 26124125]
4. Palmer AG 3rd. J Magn Reson. 2014; 241:3–17. [PubMed: 24656076]
5. Fawzi NL, Ying J, Ghirlando R, Torchia DA, Clore GM. Nature. 2011; 480:268–272. [PubMed: 22037310]
6. Fawzi NL, Ying J, Torchia DA, Clore GM. J Am Chem Soc. 2010; 132:9948–9951. [PubMed: 20604554]
7. Anthis NJ, Clore GM. Q Rev Biophys. 2015; 48:35–116. [PubMed: 25710841]
8. Neudecker P, Robustelli P, Cavalli A, Walsh P, Lundstrom P, Zarrine-Afsar A, Sharpe S, Vendruscolo M, Kay LE. Science. 2012; 336:362–366. [PubMed: 22517863]
9. Shen Y, Lange O, Delaglio F, Rossi P, Aramini JM, Liu G, Eletsky A, Wu Y, Singarapu KK, Lemak A, Ignatchenko A, Arrowsmith CH, Szyperski T, Montelione GT, Baker D, Bax A. Proc Natl Acad Sci U S A. 2008; 105:4685–4690. [PubMed: 18326625]
10. Kiser PD, Lorimer GH, Palczewski K. Acta Crystallogr, Sect F: Struct Biol Cryst Commun. 2009; 65:967–971.
11. Van der Vies SM, Viitanen PV, Gatenby AA, Lorimer GH, Jaenicke R. Biochemistry. 1992; 31:3635–3644. [PubMed: 1348956]
12. Stan G, Brooks BR, Lorimer GH, Thirumalai D. Proc Natl Acad Sci U S A. 2006; 103:4433–4438. [PubMed: 16537402]
13. Finkelstein AV. J Phys Chem B. 2015; 119:158–163. [PubMed: 25478873]
14. Braig K, Otwinowski Z, Hegde R, Boisvert DC, Joachimiak A, Horwich AL, Sigler PB. Nature. 1994; 371:578–586. [PubMed: 7935790]
15. Fitzkee NC, Rose GD. Proc Natl Acad Sci U S A. 2004; 101:12497–12502. [PubMed: 15314216]
16. Mittal J, Best RB. Proc Natl Acad Sci U S A. 2008; 105:20233–20238. [PubMed: 19073911]
17. Zhou HX, Dill KA. Biochemistry. 2001; 40:11289–11293. [PubMed: 11560476]

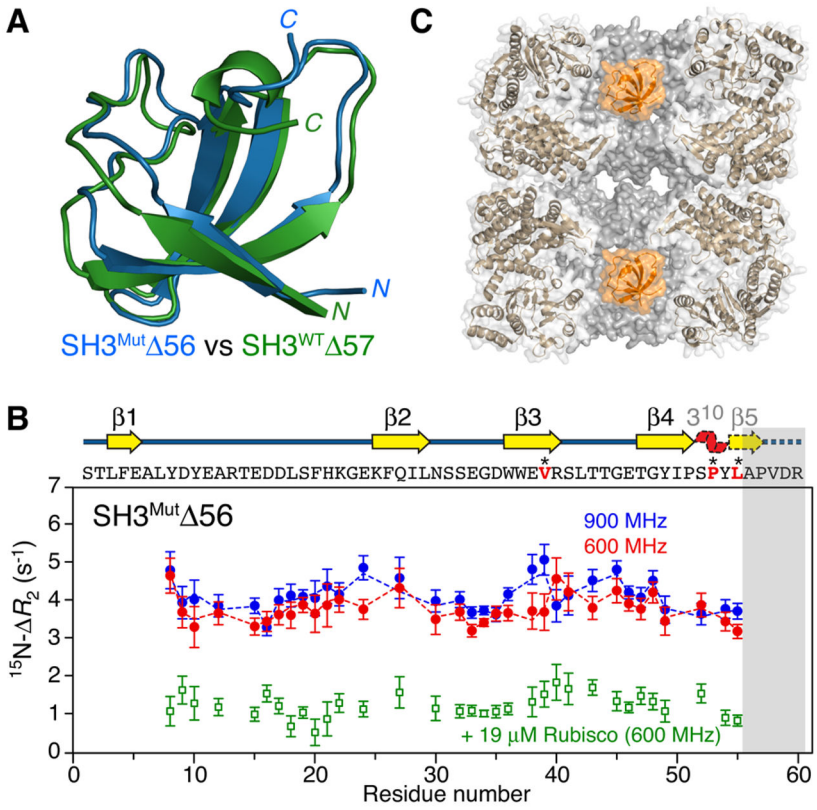

Figure 1.

Interaction of SH3^{Mut}Δ56 with apo GroEL. (A) Ribbon diagrams showing a superposition of the structures of SH3^{Mut}Δ56 (blue) and SH3^{WT}Δ57 (green), representing mimetics of a folding intermediate of the Fyn SH3 domain, determined from backbone chemical shifts and residual dipolar couplings using CS-Rosetta[9] (see the Supporting Information and Figures S2 and S3). (B) ^{15}N ΔR_2 observed for 100 μM ^{15}N-labeled SH3^{Mut}Δ56 in the presence of 120 μM (in subunits) apo GroEL at 900 MHz (blue circles) and 600 MHz (red circles) and 10 °C. The dashed lines represent the best fits obtained by simultaneously fitting all relaxation data (ΔR_2, DEST, and relaxation dispersion) to the model shown in Figure 3. The ΔR_2 effect is essentially abolished when the GroEL cavity is blocked by acid-denatured Rubisco (green circles). The gray bar indicates the residues deleted in SH3^{Mut}Δ56. The sequence (residues in red are sites of mutations) and secondary structure are shown above the panel; the 3^{10} helix and β5 (dashed outline) are unfolded in SH3^{Mut}Δ56, but only β5 is unfolded in SH3^{WT}Δ57 (see panel A). Error bars are one standard deviation. (C) Cross section through apo GroEL (Protein Data Bank entry 3E76[10]) illustrating the two cavities with a SH3^{Mut}Δ56 molecule (orange, space-filling model) confined in each cavity.

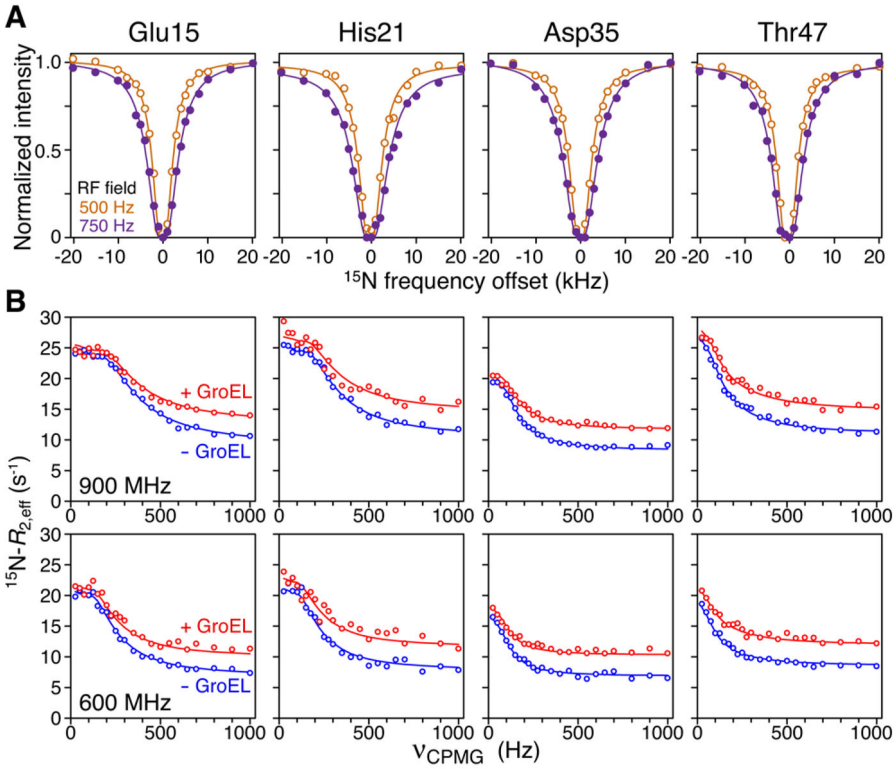

Figure 2.

^{15}N DEST and CPMG relaxation dispersion observed for 100 μM ^{15}N-labeled SH3^{Mut}Δ56 in the presence of 120 μM (in subunits) apo GroEL at 10 °C. (A) Examples of ^{15}N DEST profiles at RF field strengths of 500 MHz (orange circles) and 750 MHz (purple circles). (B) Examples of ^{15}N CPMG relaxation dispersion curves in the presence (red circles) and absence (blue circles) of apo GroEL at 900 MHz (top) and 600 MHz (bottom). The solid lines represent best fits obtained by simultaneously fitting all relaxation data (ΔR_2, DEST, and relaxation dispersion) to the model shown in Figure 3.

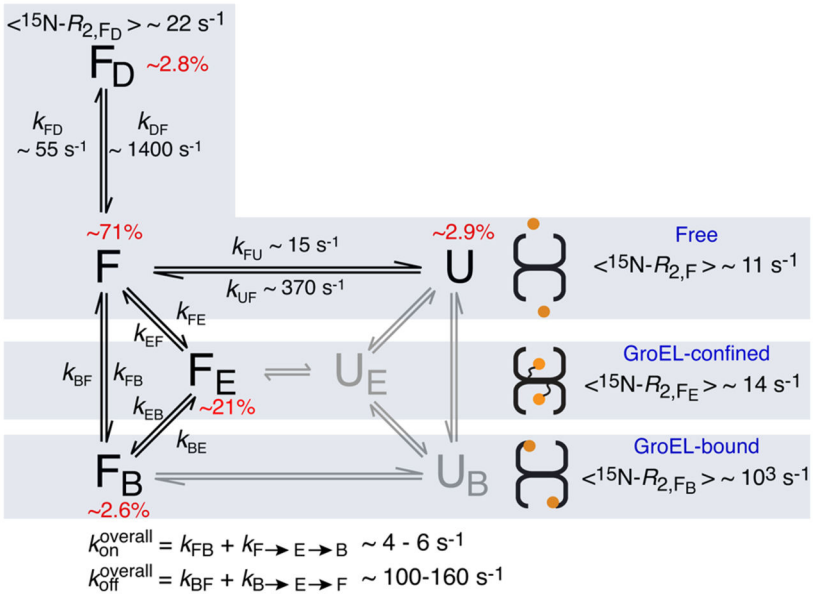

Figure 3.

Kinetic scheme for the interaction of $SH3^{Mut}\Delta56$ with apo GroEL. The populations of states U_E and U_B, colored gray, are below the limits of detection and were therefore not included in the fitting of the relaxation data (see the Supporting Information for theory and details of the fitting procedure). The rate constants and populations relate to experimental conditions of 100 μM SH3 domain and 120 μM (in subunits) GroEL at 10 °C. Binding of the dimer F_D to GroEL is assumed to be undetectable because of both its size and the fact that dimerization occludes the GroEL-binding surface (Figure S6). For $SH3^{WT}\Delta57$, there is no evidence of the existence of an unfolded state as no relaxation dispersion is observed. The ^{15}N ΔR_2 and DEST data for $SH3^{WT}\Delta57$ (Figure S7) show binding of the folded state to GroEL and are explained by two-state exchange between states F and F_B, with k_{FB} and k_{BF} values of ~7 and 500 s^{-1}, respectively (corresponding to p_B ~ 1.4%).